

## ARTICLE

# Pharmacological characterization of a clinical candidate, TG-0054, a small molecule inverse agonist targeting CXCR4



Kylie S. Pan <sup>1,2</sup> , Ziming Wang <sup>3</sup> , Cy Pfeil <sup>2</sup> , Nick D. Bergkamp <sup>2</sup> , Simon Mobach <sup>2</sup>, Susanne Roth <sup>1</sup>, Aurélien Rizk <sup>1</sup>, Martin J. Lohse <sup>3</sup>, Paolo Annibale <sup>3,4</sup> , Marco Siderius <sup>2</sup> , Mirjam Zimmermann <sup>1</sup>, Martine J. Smit <sup>2</sup>, Reggie Bosma <sup>2,\*</sup>

<sup>1</sup> InterAx Biotech AG, Villigen, Switzerland

<sup>2</sup> Division of Medicinal Chemistry, Faculty of Sciences, Department of Chemistry and Pharmaceutical Sciences, Amsterdam Institute of Molecular and Life Sciences (AIMMS), Vrije Universiteit Amsterdam, Amsterdam, The Netherlands

<sup>3</sup> Max Delbrück Center for Molecular Medicine in the Helmholtz Association, Berlin, Germany

<sup>4</sup> School of Physics and Astronomy, University of St Andrews, St Andrews, United Kingdom

## ARTICLE INFO

## Article history:

Received 8 July 2024

Accepted 8 January 2025

Available online 31 January 2025

## Key words:

cAMP

Chemokine receptors

G protein-coupled receptors

Signal transduction

CXCR4

## ABSTRACT

CXCR4 is an important therapeutic target for hematopoietic stem cell mobilization, which enhances the success of autologous stem cell transplantation for treating blood cancers such as lymphomas and myeloma. As CXCR4 has been shown to be involved in various inflammatory diseases, cancer progression, and cell entry by the human immunodeficiency virus, understanding the molecular mechanism of CXCR4 inhibitors has potential implications in a wide area of diseases. Here, we present an exploratory study which involves the molecular pharmacological characterization of TG-0054 (burixafor, GPC-100), a clinical candidate for hematopoietic stem cell mobilization. TG-0054 inhibited CXCL12 binding at CXCR4, and antagonized both  $G\alpha_i$  and  $\beta$ -arrestin2 recruitment as well as the downstream  $G\alpha_i$ -attenuation of cAMP signaling pathway, with  $pIC_{50}$  of 7.7, 8.0, and 7.9, respectively. Compared with the clinically used antagonist AMD3100 and the prototypical inverse agonist Isothiourea-1t (IT1t), TG-0054 displayed a unique pharmacological profile. Like IT1t, TG-0054 inhibited the constitutive  $G\alpha_i$  signaling of CXCR4. However, in contrast to IT1t and other reported inverse agonists, TG-0054 was not able to induce monomerization of CXCR4 oligomeric complexes. Considering the unique properties of TG-0054 on CXCR4, TG-0054 is an interesting tool compound for studying the relevance of inverse agonism as well as CXCR4 monomerization in various pathologies.

**Significance Statement:** CXCR4-targeted therapeutics hold important potential for the treatment of blood cancers. TG-0054 has inverse agonistic properties and is a non-CXCR4-monomerizing small molecule antagonist, unlike other well studied CXCR4 small molecule antagonists.

© 2025 The Authors. Published by Elsevier Ltd. This is an open access article under the CC BY license (<http://creativecommons.org/licenses/by/4.0/>).

## 1. Introduction

CXCR4 is a class A G protein-coupled receptor (GPCR) from the chemokine receptor family with CXCL12 as its endogenous ligand (Bachelierie et al, 2014). It plays important roles in cell migration,

\* **Address correspondence to:** Dr Reggie Bosma, Division of Medicinal Chemistry, Faculty of Sciences, Department of Chemistry and Pharmaceutical Sciences, Amsterdam Institute of Molecular and Life Sciences (AIMMS), Vrije Universiteit Amsterdam, De Boelelaan 1108, 1081 HZ Amsterdam, The Netherlands. E-mail: [r.bosma@vu.nl](mailto:r.bosma@vu.nl)

 This article has supplemental material available at [molpharm.aspetjournals.org](http://molpharm.aspetjournals.org).

development, inflammation, and cancer progression, and functions as a coreceptor for the cellular entry of HIV (Heuninck et al, 2019; Bachelierie et al, 2020; Pándy-Szekeres et al, 2023). In the clinic, CXCR4 antagonist AMD3100 (plerixafor) is used to induce hematopoiesis, in which hematopoietic stem cells (HSCs) migrate out of the bone marrow to give rise to mature blood cells (Murdoch, 2000). In the treatment of blood cancers such as multiple myeloma, Hodgkin's disease, or non-Hodgkin's lymphoma, mobilization of HSC is especially important, as the mature blood cells are collected from patients for autologous HSC transplantation and a high yield is often needed for successful transplantation (Copelan, 2006). HSC retention in the bone marrow was shown to be caused by CXCL12-mediated activation of CXCR4- $G_i$  signaling (Moll



### 2.3. Cell culture

HEK293 cells (RRID:CVCL\_0045) were cultured in DMEM supplemented with 10% FBS at 37 °C and in a humidified atmosphere with 5% CO<sub>2</sub>. HEK293T cells (RRID:CVCL\_0063) were cultured in the same condition, with 100 U/mL penicillin and 100 µg/mL streptomycin added to medium. HEK293AD cells were cultured in the same condition, with 2 mM L-glutamate, 100 U/mL penicillin, and 100 µg/mL streptomycin added to medium. SNAP-CXCR4 expressing HEK293 cells used in CXCL12 displacement experiments were purchased from Revvity (C1SU1CXCR4) and cultured similarly with 1 mg/mL G418 added to culture medium. Stable cell lines (SNAP-CXCR4 and/or EPAC expressing) were generated in a HEK293 background. HEK293 cells were transfected with 8 µg plasmid DNA and 24 µL of lipofectamine 2000 in 10-cm dishes and selected with 2 mg/mL G418 and/or 0.2 mg/mL Zeocin for 7 days. After selection, cells were labeled with SNAP-488 and sorted via fluorescence-activated cell sorter into single cells, which were clonally expanded. Stable cell lines with CXCR4 and/or EPAC integration were cultured similarly, with 1 mg/mL G418 and/or 0.06 mg/mL Zeocin added to culture medium.

### 2.4. Transient transfection of HEK293 cells

HEK293 cells were detached with 1 mL Versene per T75 flask and were seeded at  $3 \times 10^4$  cells per well. The next day, cells were incubated for 30 minutes in Opti-MEM before a 5-hour incubation with a transfection mixture containing 0.1 µg plasmid DNA and 0.1 µL of lipofectamine 2000 at 37 °C 5% CO<sub>2</sub>. Cells were then recovered overnight with DMEM containing 10% FBS, and were used in assays the following day. Transfection conditions for other cell types (HEK293AD, HEK293T) used are described in the corresponding experimental methods sections.

### 2.5. Whole cell ligand binding to CXCR4

To detect binding of CXCL12-AZ647 to SNAP-CXCR4, HEK293 cells stably expressing SNAP-CXCR4 were seeded into poly-L-Lysine coated white 96-well plates at  $3 \times 10^4$  cells per well in DMEM with 10% FBS and grown for 24 hours. Growth medium was aspirated and the cells were first labeled with SNAP-Lumi-Tb for 1 hour at 4 °C to label surface-expressed CXCR4. Then, unbound SNAP-Lumi-Tb was removed and cells were incubated in HBSS with 20 mM Hepes and 0.1% bovine serum albumin (BSA) at room temperature for 15 minutes. The relative levels of CXCR4-bound CXCL12-AZ647 were then measured using the PHERAstar in homogeneous time resolved fluorescence (HTRF) mode for up to 30 minutes at 25 °C. HEK293 cells expressing SNAP-H1 were used to control for the extent of nonspecific binding. A one-site total binding model was used in GraphPad Prism (GraphPad), to determine the pK<sub>d</sub> of CXCL12-AZ647 at SNAP-CXCR4.

Displacement of CXCL12-AZ647 from SNAP-CXCR4 by TG-0054, AMD3100, and IT1t was tested by seeding SNAP-CXCR4-expressing HEK293 cells (Revvity) into poly-D-Lysine coated 96-well Opti-Plates at  $5 \times 10^4$  cells per well in DMEM with 10% FBS and incubating for 48 hours. Growth medium was aspirated and the cells were first labeled with SNAP-Lumi-Tb for 1 hour at 37 °C 5% CO<sub>2</sub> to label surface-expressed CXCR4, unbound SNAP-Lumi-Tb was removed by washing the cells with HBSS, and cells were subsequently incubated with TG-0054, IT1t, or AMD3100 (10 µM–0.001 nM) and CXCL12-AZ647 (10 nM) in HBSS with 20 mM Hepes and 0.1% BSA at room temperature and 300 rpm. The level of nonspecific CXCL12-AZ647 binding was assessed by measuring fluorescence readout after using 10 mM of AMD3100 to saturate CXCL12 binding sites on CXCR4. The relative levels of CXCR4-bound

CXCL12-AZ647 were then measured using the PHERAstar in HTRF mode for up to 45 minutes at 25 °C.

### 2.6. BRET-based miniGαi and β-arrestin recruitment

CXCR4-NLuc and mVenus/Venus-tagged effectors were transfected as described in [Transient Transfection of HEK293 Cells](#). On the day of the experiment, growth medium was aspirated, and cells were washed with PBS. TG-0054, IT1t, and AMD3100 (1 mM–0.001 nM) were diluted in assay buffer (HBSS with 20 nM Hepes and 0.1% BSA) were applied for 30 minutes at 37 °C 5% CO<sub>2</sub>. Cells were stimulated with an additional 10 nM CXCL12 for 15 minutes and 1:1000 diluted Nano-Glo substrate (furimazine) was added to all wells before readout on the PHERAstar using optical module fl 430 480 520 at 25 °C.

BRET ratio was calculated with in-built ratio calculator in MARS (BMG LABTECH) using the following equation:

$$\text{Ratio} = \text{Emission}_{\text{Acceptor}} \div \text{Emission}_{\text{Donor}}$$

with emission signal of acceptor at 520 nm and that of donor at 480 nm.

### 2.7. cAMP measurement

cAMP levels in HEK293 cells were measured as described previously ([Mathiesen et al, 2013](#); [Benkel et al, 2022](#)). EPAC-based FRET sensor was introduced into CXCR4 overexpressing HEK293 cells as described in transient transfection of HEK293 cells. On the day of the experiment, the plate with cells was first equilibrated to room temperature for 25 minutes. The plate was then placed in PHERAstar and read in kinetic fluorescence mode with the fl 430 480 520 module at 25 °C. Modulators were added uniformly using VIAFLO 96. FSK (6.3 µM) was supplied simultaneously to treated wells in cycle 3. CXCL12 (2 nM) was added at cycle 15, and TG-0054, AMD3100, and IT1t (50 µM–2 nM) were added at cycle 42 of the measurement. FRET signal was analyzed as donor emission over acceptor emission. On cAMP binding, the sensor changes to an open conformation resulting in the loss of FRET, increasing emission from donor.

### 2.8. Receptor oligomerization of CXCR4-Rluc and CXCR4-YFP in HEK293T cells

A total of  $1 \times 10^6$  cells HEK293T cells were transfected using 6 µg 25-kDa linear PEI and 1 µg of DNA, consisting of 40 ng Myc-CXCR4-Rluc pIRES, 400 ng HA-CXCR4-YFP pIRES and 560 ng empty pcDEF3 vector. The DNA-PEI mixture was prepared in 150 mM NaCl and vortexed for 3 seconds. During 15-minute incubation of the DNA-PEI mixture at room temperature, cells were detached with trypsin and resuspended in DMEM. The HEK293T cell suspension was added to the DNA-PEI mixture, and cells were then seeded at  $3.5 \times 10^4$  per well in white flat-bottom 96-well plates. After 48-hour incubation, cells were washed once using PBS and maintained in HBSS supplemented with 0.1% BSA, 1 mM MgCl<sub>2</sub>, and 2 mM CaCl<sub>2</sub>. Cells were stimulated with increasing concentrations of CXCL12, AMD3100, TG-0054, or IT1t for 15 minutes before BRET measurements. After incubating cells for 10 minutes with 5 µM coelenterazine-h substrate, bioluminescence was measured at 535/30 nm and 475/30 nm using a PHERAstar plate reader. BRET signals were determined as the ratio of luminescence in the acceptor channel (535/30 nm) divided by the donor channel (475/30 nm). The ligand-promoted BRET signal was normalized by dividing BRET values by the reference BRET values measured for vehicle-treated cells.

### 2.9. SpIDA and TB analysis for determining GPCR oligomeric state in HEK293AD cells

Procedures were carried out as described earlier in Nature Protocols in detail (Işbilir et al., 2021). Briefly,  $3 \times 10^5$  HEK293AD cells were seeded on 24 mm ( $\emptyset$ ) round glass coverslips, cultured in DMEM supplemented with 10% FBS (vol/vol), 2 mM L-glutamate, 100 U/mL penicillin, and 100  $\mu$ g/mL streptomycin at 37 °C and in a humidified atmosphere with 5% CO<sub>2</sub>. Cells were detached with trypsin. After an overnight incubation, cells were transfected with a 1 mL mixture containing 0.6  $\mu$ g constructs expressing CXCR4-EYFP or  $\beta_1$ AR-EYFP together with 1.8  $\mu$ L lipofectamine 2000 in Opti-MEM medium. Cells were transfected overnight. Then the coverslip with transfected cells was mounted onto the Attofluor chamber and washed 3 times with 500  $\mu$ L HBSS, after which cells were reconstituted in 450  $\mu$ L HBSS before imaging. For the ligand treatment, 10  $\mu$ M was used as the final concentration of IT1t or TG-0054 for the 30-minute incubation at 37 °C prior to imaging.

Images for SpIDA and TB were acquired with a commercial laser-scanning confocal microscope (Leica SP8) with an oil-immersion objective (HC PL APO CS2 40 $\times$ /1.25NA). Excitation was provided by a white light laser, and emission was collected using photon counting hybrid detectors. The excitation laser line used was at 514 nm, and the emission band was set for 520–600 nm. The imaging setting was in a xyt mode. For spatial brightness measurements, images were captured at 512  $\times$  512 pixels with a 50-nm pixel size in 16-bit format. The scanner speed was set to 100 Hz using a 15% laser power. For TB, images were captured at 256  $\times$  256 pixels with a 50-nm pixel size in 8-bit format. The scanner speed was set to 400 Hz using a 2% laser power. In total, 100 frames were captured with a time interval of 1 second between frames.

### 2.10. Data analysis

For BRET signals, pIC<sub>50</sub> determination was carried out on raw data using log(inhibitor) versus response (3-parameter) in-built in Prism 9.3.1.

$$Y = Bottom + (Top - Bottom) / \left( 1 + 10^{(\text{LogIC}_{50} - X) * \text{Hillslope}} \right)$$

where Y is response and X represents log [ligand concentration]. Bottom of AMD3100 curve in  $\beta$ -arrestin recruitment was constrained to background levels of BRET (no stimulation), as its bottom plateau was not well defined. pIC<sub>50</sub> corresponds to the concentration of ligand required to inhibit 50% of maximal response. pIC<sub>50</sub> values from individual experiments were calculated, and then averaged. BRET ratios were normalized to the maximal value in each experiment and combined to present as data summary.

For kinetic traces, normalization was carried out by subtracting traces recorded in the buffer-only condition from ligand-treated conditions. Concentration-dependent inhibition curves of CXCR4 ligands (from inhibitor addition to 120 minutes) were calculated by integrating the area under the curve (AUC). The raw AUC values from each ligand's biological repeat (N) were normalized and expressed as % of the highest maximal AUC value induced by 1 of the 3 ligands tested in parallel (TG-0054, IT1t, and AMD3100). Similarly, the lowest minimal AUC value was set to 0%. In case the ligand (ie, AMD3100) had an inhibitory effect on cAMP levels (implying CXCR4 agonism) normalization was adjusted by setting 0% and –100% to the highest AUC and lowest AUC, respectively. Nonlinear regression was carried out using log(inhibitor) versus

response (3-parameter) in-built in Prism 9.3.1., top constrained to 100, bottom constrained to 0.

$$Y = Bottom + (Top - Bottom) / \left( 1 + 10^{(\text{LogIC}_{50} - X) * \text{Hillslope}} \right)$$

where Y is response and X represents log [ligand concentration]. pIC<sub>50</sub> corresponds to the concentration of ligand required to inhibit 50% of maximal response. pIC<sub>50</sub> values from individual experiments were calculated, and then averaged.

Confocal microscopy images used for SpIDA were additionally converted into 16 bit in Fiji; those used for TB were converted into 8 bit. Images were then imported into IgorPro9, and regions of interest (ROI) were selected as previously mentioned (for stepwise workflow, see Annibale and Lohse, 2020; Işbilir et al., 2021). At least 6 ROIs were selected for each image. The photon count and its SD were used to calculate molecular brightness ( $\epsilon$ ), which was compared with the value of the monomeric control ( $\beta_1$ AR-EYFP) to determine the oligomeric state of CXCR4-EYFP. Analysis protocol for IgorPro is deposited by Dr Paolo Annibale at <https://github.com/PaoloAnnibale/Mole-cularBrightness> and reported by Işbilir et al (2021). Statistical significance testing was done by one-way ANOVA followed post hoc by Tukey's multiple pairwise comparison.

## 3. Results

### 3.1. TG-0054 displaces CXCL12 binding at CXCR4

To determine the inhibitory potency of TG-0054 for CXCR4, we generated a stable cell line expressing SNAP-tagged CXCR4 and used an HTRF-based binding assay using fluorescently labeled (AZ647) CXCL12, detecting binding of CXCL12-AZ647 to SNAP-CXCR4 with a pK<sub>d</sub> of  $7.8 \pm 0.3$  (Supplemental Fig. 1). As shown in Fig. 2A, AMD3100, TG-0054, and IT1t were all able to displace CXCL12-AZ647. TG-0054 displaced CXCL12-AZ647 binding at CXCR4 with a pIC<sub>50</sub> of  $7.4 \pm 0.2$ , similar to the inhibitory potency of IT1t (pIC<sub>50</sub> =  $7.4 \pm 0.2$ ) (Fig. 2B). TG-0054 has therefore an inhibitory potency for CXCL12-CXCR4 binding comparable to IT1t and higher than AMD3100 (Table 1).

### 3.2. TG-0054 inhibits CXCL12-induced G $\alpha_i$ and $\beta$ -arrestin2 recruitment to CXCR4

Next, we examined whether displacement of CXCL12 by TG-0054 translates into inhibition of G $\alpha_i$  and  $\beta$ -arrestin2 recruitment. These 2 effectors are known to propagate signaling downstream of CXCR4 activation (Heuninck et al., 2019). BRET between miniG $\alpha_i$  (Venus-tagged) or  $\beta$ -arrestin2 (mVenus-tagged) and CXCR4 (tagged with NLuc) was measured. CXCL12 induced recruitment of both effectors to CXCR4 in a dose-dependent manner (Supplemental Figs. 2 and 3). TG-0054, AMD3100, and IT1t were able to reduce CXCL12-induced miniG $\alpha_i$  or  $\beta$ -arrestin2 recruitment to the CXCR4 in a dose-dependent manner back to basal level (Fig. 3; Supplemental Figs. 2 and 3). TG-0054 has a pIC<sub>50</sub> of  $7.7 \pm 0.2$  and  $8.0 \pm 0.1$  for miniG $\alpha_i$  and  $\beta$ -arrestin2, respectively. These inhibitory potencies are similar to that of IT1t ( $7.4 \pm 0.2$  and  $7.7 \pm 0.2$ ) but higher than those of AMD3100 ( $6.7 \pm 0.1$  and  $6.6 \pm 0.1$ ).

### 3.3. TG-0054 inhibits CXCL12 mediated and constitutive signaling by CXCR4

Next, we measured G $\alpha_i$ -dependent CXCR4 signaling in real time to study the effect of TG-0054 on the receptor. As a signal readout, we measured cAMP levels in the cell population using a FRET-based

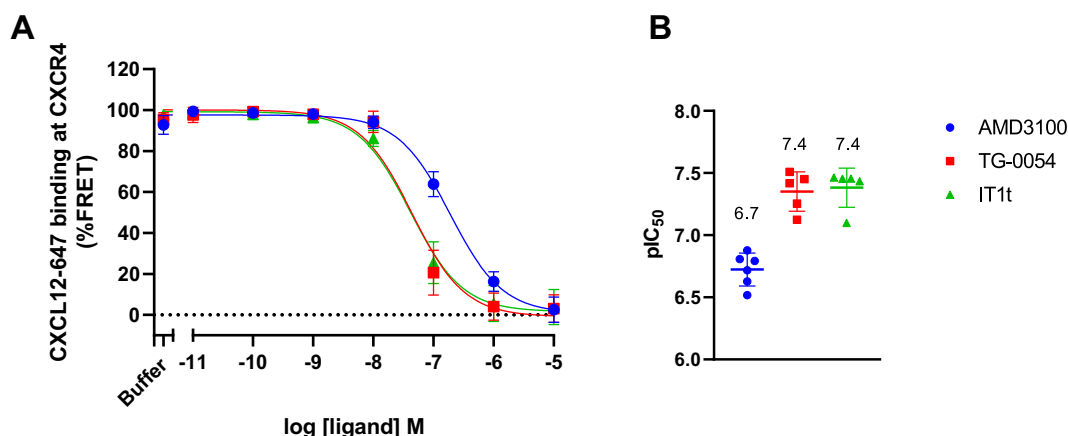


**Fig. 2.** Displacement of CXCL12-AZ647 at CXCR4 by unlabeled ligands. HEK293 cells stably expressing SNAP-CXCR4 were labeled with SNAP-LumiITb, and then incubated with 10 nM CXCL12-AZ647 and increasing concentrations of inhibitors. (A) Binding curve shows  $N = 6$  experiments (AMD3100),  $N = 5$  experiments (TG-0054, IT1t), data points reflect the mean  $\pm$  SD of normalized and combined data and fitted with one-site binding equation for illustrative purposes. Data are normalized per experiment to fluorescent CXCL12 only (10 nM CXCL12-AZ647 = 100%) and to full displacement of CXCL12 (10 nM CXCL12-AZ647 + 10  $\mu$ M AMD3100 = 0%). Raw fluorescence (before normalization) ranged between 640,416 and 43,275 counts at 337/665 nm and between 1114,422 and 389,305 at 337/620 nm with the BRET ratio ranging between 0.710476 and 0.07885. (B) Comparisons of pIC<sub>50</sub> values determined for TG-0054, AMD3100, and IT1t, with mean  $\pm$  SD depicted.

EPAC sensor (Mathiesen et al, 2013) in HEK293 cells stably expressing CXCR4. In Fig. 4, it was shown that cells treated with FSK (6.3  $\mu$ M) have elevated cAMP accumulation, which was decreased by a subsequent stimulation of the CXCR4-G $\alpha_i$  pathway with 2 nM CXCL12. All 3 inhibitors AMD3100, TG-0054, and IT1t were able to reverse the CXCL12-mediated attenuation of cAMP in a concentration-dependent manner (Fig. 4). TG-0054 had a pIC<sub>50</sub> of  $7.9 \pm 0.2$ , which is again in the same range as that of IT1t ( $8.0 \pm 0.3$ ), whereas AMD3100 has the least potent receptor inhibition ( $6.6 \pm 0.1$ ).

Interestingly, in the absence of CXCL12, both TG-0054 and IT1t induced a small increase in cAMP levels, which was not observed on treatment with AMD3100 (Fig. 5, A–C). As CXCR4 is known to exhibit increased basal activity in certain contexts (Işbilir et al, 2020; Smit et al, 2021), the ligand-induced increase in cAMP levels likely reflects its inverse agonism on basal CXCR4 signaling. To better observe and quantify the inverse agonism of TG-0054, we took advantage of a constitutively active mutant of CXCR4, CXCR4-N119S (Zhang et al, 2002), an often-used approach to study the inverse agonism of GPCR ligands (Wade et al, 2001; Brillet et al, 2003). HEK293 cells were transiently transfected with CXCR4-N119S and EPAC sensor. The EPAC sensor showed the expected increase in cAMP levels upon treatment with FSK (Fig. 5, D–F). The known inverse agonism of CXCR4 by IT1t was confirmed (Fig. 5, F–H; Supplemental Fig. 4), with a pIC<sub>50</sub> of  $7.7 \pm 0.1$ . In agreement with previous reports (Rosenberg et al, 2019), AMD3100 behaved as a partial agonist of CXCR4-N119S (Fig. 5, D and G). A clear dose-dependent increase in cAMP levels was visible upon subsequent treatment with TG-0054 (Fig. 5, E, G, and H), implying inhibition of basal CXCR4 signaling with a pIC<sub>50</sub> of  $7.5 \pm 0.2$ . These results confirm that indeed, like IT1t, TG-0054 is an inverse agonist of CXCR4<sup>N119S</sup>, thus corroborating that the observed increases in Fig. 5, A–C are also due to inverse agonism on wild-type CXCR4.

### 3.4. TG-0054 does not monomerize CXCR4

CXCR4 has been reported to exist as homodimers, which can be disrupted by inverse agonists like IT1t (Işbilir et al, 2020; Ward et al, 2021). Because our data show that both TG-0054 and IT1t inhibit the basal activity of CXCR4 (Fig. 5), we were interested to see whether TG-0054 also induces the same effect on CXCR4 oligomeric states as IT1t. First, we analyzed the proximity of CXCR4 receptors using a BRET-based assay. HEK293T cells were transiently transfected with 2 plasmids encoding CXCR4 fused at the C-terminus with either a BRET donor (Rluc) or acceptor (YFP). CXCL12 induced a dose-dependent increase in BRET signal, suggesting the further induction of oligomerization of the receptor (Fig. 6A), in line with published data (Percherancier et al, 2005). AMD3100 did not affect CXCR4 clustering BRET, whereas IT1t disrupted CXCR4 clustering shown by a dose-dependent decrease in BRET. Surprisingly, TG-0054 showed a small dose-dependent increase in CXCR4 clustering, in contrast to what is known for other inverse agonists of the CXCR4 (Işbilir et al, 2020; Ward et al, 2021).

To further confirm the effect of TG-0054 on CXCR4 oligomer disruption, we performed another microscopy-based single-cell molecular brightness analysis to determine the oligomeric states of CXCR4. The technique hinges on the molecular brightness which is defined by the fluctuation in the number of photons detected either at different time points in individual pixels (TB) or in different positions of the same homogenous region (SpIDA) (for detailed analysis protocol, see Işbilir et al, 2021). The measured brightness can be used to quantify molecular oligomerizations because the molecular brightness of a fluorescent oligomer is linearly dependent on the number of its labeled protomers (see Supplemental Fig. 5 for representative images used for analysis). In our experiments, we used the EYFP labeled  $\beta_1$ -adrenergic receptor ( $\beta_1$ AR-EYFP) as a control, as previously reported (Işbilir et al, 2021). As

**Table 1**  
Summary of pIC<sub>50</sub> values, data reflect mean  $\pm$  SD, number of experiments indicated in brackets

	Displacement pIC <sub>50</sub>	miniG <sub>i</sub> Recruitment pIC <sub>50</sub>	$\beta$ -arr2 Recruitment pIC <sub>50</sub>	cAMP WT pIC <sub>50</sub>	cAMP CAM pIC <sub>50</sub>
AMD3100	6.7 $\pm$ 0.1 (6)	6.7 $\pm$ 0.1 (4)	6.6 $\pm$ 0.1 (5)	6.6 $\pm$ 0.1 (6)	–
TG-0054	7.4 $\pm$ 0.2 (5)	7.7 $\pm$ 0.2 (5)	8.0 $\pm$ 0.1 (5)	7.9 $\pm$ 0.2 (5)	7.5 $\pm$ 0.2 (4)
IT1t	7.4 $\pm$ 0.2 (5)	7.3 $\pm$ 0.2 (5)	7.7 $\pm$ 0.2 (5)	8.0 $\pm$ 0.3 (4)	7.7 $\pm$ 0.1 (3)

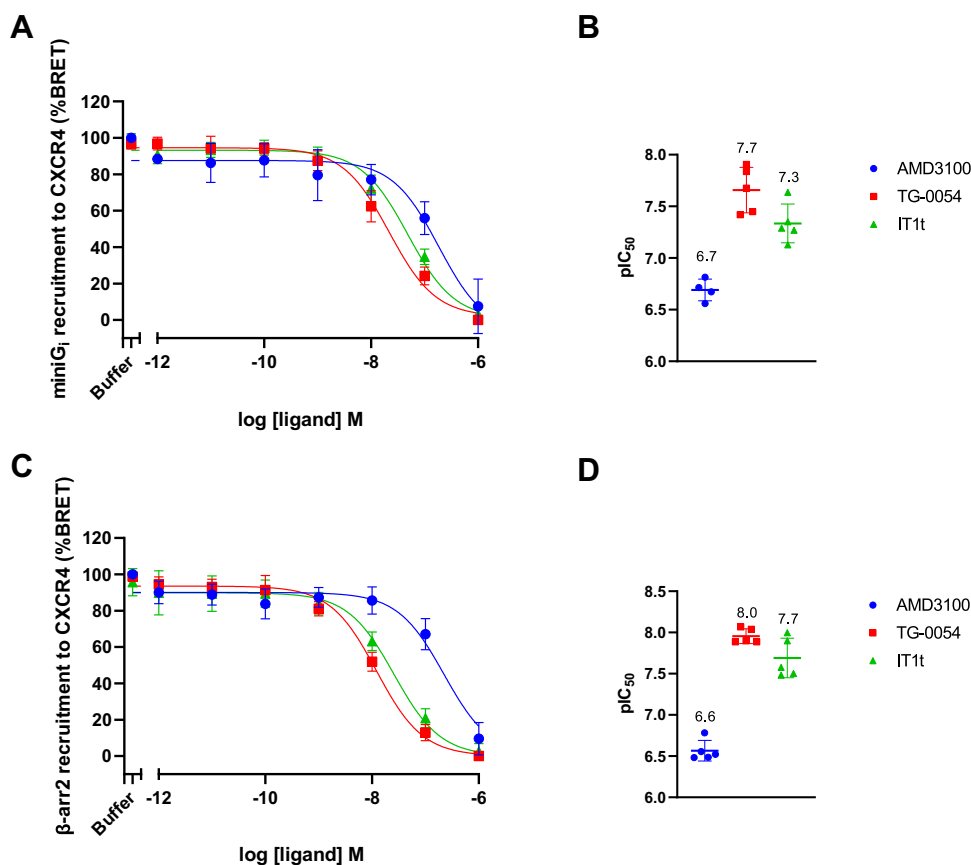


**Fig. 3.** Inhibition of CXCL12-induced CXCR4 activation by AMD3100, TG-0054, and IT1t. HEK293 cells were transiently transfected with CXCR4-NLuc and either Venus-miniG $\alpha_i$  or mVenus- $\beta$ -arrestin2. Cells were treated with 10 nM CXCL12 in the presence of increasing concentrations ligand for 15 minutes at 37 °C. (A and C) BRET ratio changes reflecting recruitment of Venus-miniG $\alpha_i$  (A) or mVenus- $\beta$ -arrestin2 (C) analysed with nonlinear curve fitting of dose response with log[inhibitor] vs response of  $N = 5$  experiments except for AMD3100 in miniG $\alpha_i$  recruitment ( $N = 4$ ), data points reflect the mean  $\pm$  SD of the normalized (10 nM CXCL12 only = 100%, no CXCL12 = 0%, for complete CXCL12 curves see Supplemental Figs. 2 and 3) and combined dataset, fitted for illustrative purposes. Note that for AMD3100, the bottom of the fitted curve was constrained to 0%. B (Venus-miniG $\alpha_i$ ), D (mVenus- $\beta$ -arrestin2): Comparisons of pIC<sub>50</sub> values determined for TG-0054, AMD3100, and IT1t, with mean  $\pm$  SD depicted.

shown in Fig. 6B (SpIDA) and Fig. 6C (TB), incubation of 10  $\mu$ M IT1t reduced the overall oligomeric state of CXCR4 closer to that of the  $\beta_1$ -adrenergic receptor. CXCR4 oligomeric states, however, did not significantly change after a 10  $\mu$ M TG-0054 treatment compared with the untreated samples. Next, to examine the consistency of obtained data using 2 different methods, the SpIDA and TB results were correlated. Indeed, the level of GPCR oligomerization that was detected using both types of analysis overlapped reasonably well as the correlation line has a slope close to 1 ( $R = 0.69$ , slope = 0.94), as depicted in Fig. 6D. This agrees with prior data, showing a correlation between both techniques to detect the oligomerization of CXCR4 in a larger dataset as well (Işbilir et al, 2020). Therefore, we could confidently detect ligand-modulated CXCR4 oligomeric states, and the results further supported the notion that TG-0054 does not disrupt the basal CXCR4 dimeric complexes.

#### 4. Discussion

In this study, we characterized the pharmacological properties of the drug candidate TG-0054. We showed that TG-0054 inhibits CXCL12 binding to CXCR4 (pIC<sub>50</sub> = 7.4  $\pm$  0.2; Fig. 2), as well as CXCL12-induced receptor activation measured by downstream CXCR4 signaling events (Figs. 3 and 4), with pIC<sub>50</sub> values ranging from 7.5 to 8.0 (Table 1). These data are in line with the reported antagonism of TG-0054 on CXCR4, describing inhibition of CXCL12-induced Ca<sup>2+</sup> signaling and cell migration (Harms et al, 2020;

Sukhtankar et al, 2023b). Moreover, we showed that TG-0054, like IT1t, inhibits the constitutive activity of CXCR4, both at the wild-type receptor (Fig. 5, A–C; Supplemental Fig. 4) and the constitutively active mutant CXCR4<sup>N119S</sup> (Fig. 5, D–F). TG-0054, therefore, was shown to modulate CXCR4 functionality in a similar fashion as IT1t, with comparable inhibitory potencies (IT1t: pIC<sub>50</sub> = 7.4–8.0). Conversely, AMD3100 was marked by a lower inhibitory potency (AMD3100: pIC<sub>50</sub> = 6.6–6.7) without any observed inverse agonism, in line with published data (Sukhtankar et al, 2023b).

Despite similarities, TG-0054 also showed some unique pharmacological properties compared with IT1t, as TG-0054 did not monomerize CXCR4 (Fig. 6). TG-0054 was shown to induce an apparent increase in CXCR4 clustering as measured with the BRET sensors (Fig. 6A), whereas SpIDA and TB analysis indicated that TG-0054 did not affect the clustering of CXCR4 (Fig. 6, B–D), which is constitutively largely dimeric. As BRET levels are not solely dependent on the proximity between receptors but might also reflect differences in receptor conformations, we would argue that TG-0054 is likely to have a limited effect on receptor clustering. Moreover, BRET signal may incorporate the effects from receptors in intracellular compartments, where increased spatial proximity may mask bona fide oligomerization at the plasma membrane.

Several recent studies investigated the formation of CXCR4 dimers and oligomers. CXCR4 dimers were shown to have enhanced constitutive signaling (Işbilir et al, 2020), but it was also shown that dimerization was not essential for CXCL12-induced G protein

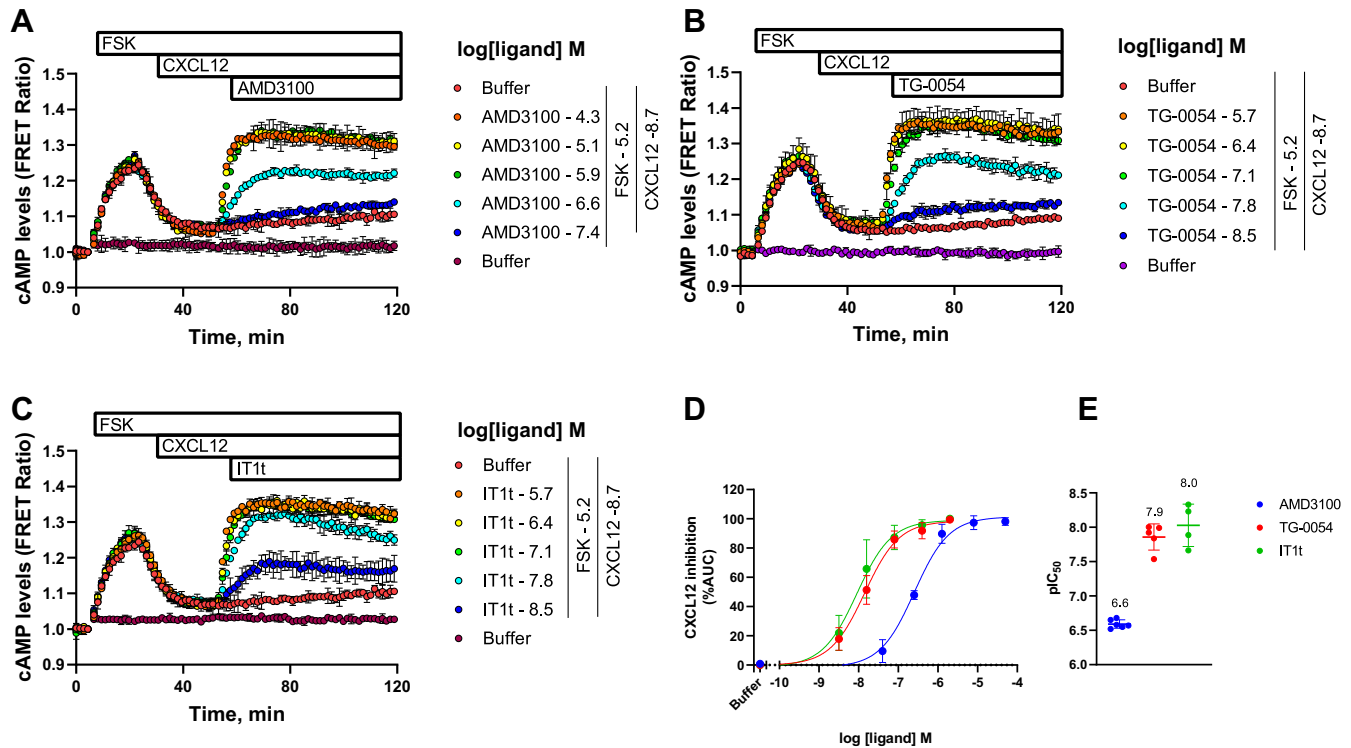


**Fig. 4.** TG-0054 inhibits CXCR4-mediated attenuation of cAMP levels. (A–C) HEK293 cells with stable SNAP-CXCR4 expression and transient transfection of EPAC FRET sensor were sequentially exposed to fixed concentrations of FSK ( $t = 7$  minutes) and 2 nM CXCL12 ( $t = 22$  minutes) then increasing concentrations of CXCR4 inhibitors ( $t = 53$  minutes). Graphs show representative traces of  $N = 6$  (AMD3100), 5 (TG-0054), and 4 (IT1t) experiments with duplicates per condition. FRET ratios were calculated as the FRET-donor signal over the FRET-acceptor signal, and the resulting signal is therefore proportional to the level of cAMP levels. (D) Dose-dependent inhibition curves of TG-0054, AMD3100, and IT1t for CXCL12 induced CXCR4 activity. Data points represent the inhibitor response ( $t = 53$ –120 minutes) of the experiments depicted in panels A–C, quantified by AUC. For each inhibitor, the values are buffer-corrected and normalized to the maximum response (buffer = 0%, max inhibitor concentration = 100%), depicted as mean  $\pm$  SD and fitted for illustrative purposes. (E) Comparisons of pIC<sub>50</sub> values determined for TG-0054, AMD3100, and IT1t, with mean  $\pm$  SD depicted.

activation by the receptor (Ward et al, 2021). IT1t and other ligands known to monomerize the receptor have been put forward as tools to investigate the functional relevance of CXCR4 dimers and oligomers. However, because all established monomerizers of the CXCR4 are also inverse agonists (İşbilir et al, 2020), it is hard to distinguish the effect of monomerization and impaired basal signaling of CXCR4 on treatment with these ligands. TG-0054 is, therefore, an interesting addition to the pharmacological toolbox as it impairs basal signaling with limited effect on CXCR4 supramolecular arrangement. Additionally, TG-0054 could provide opportunities to study complex phenotypes in which the contribution of CXCR4 is not well understood, for example in the engraftment of HSCs, which has been found in different studies to be either enhanced (Kang et al, 2010) or reduced (Kazemi et al, 2016) upon treatment with AMD3100.

CXCR4 binding of TG-0054, AMD3100, and IT1t was also studied in a different competitive binding assay, using the CXCR4 antibody 12G5 as the competitive probe, resulting in a very high inhibitory potency of TG-0054 (pIC<sub>50</sub> = 9.5, Harms et al, 2020). The inhibitory potency of TG-0054 on 12G5 binding was >100-fold higher than what is observed here for the displacement of CXCL12 in this study (pIC<sub>50</sub> = 7.4). In contrast, when comparing the IC<sub>50</sub> values for 12G5 displacement (Harms et al, 2020) with CXCL12 displacement (Fig. 2), the inhibitory potencies of IT1t and AMD3100 only differed by 27-fold and 3-fold, respectively. These probe-dependent inhibitory potencies might suggest that these small molecule inhibitors do not displace 12G5 and CXCL12 from the CXCR4 competitively and might rely on an allosteric mechanism of inhibition. In line with this hypothesis, it was recently shown that CXCL12 does not

always bind competitively with small molecule inhibitors on its receptors, CXCR4 (García-Cuesta et al, 2024) and ACKR3 (Yen et al, 2022; García-Cuesta et al, 2024).

Within the 7 transmembrane (TM) binding pockets of CXCR4, AMD3100 and IT1t have been reported to have distinct binding interactions, in which IT1t is binding closer to TM domain 2 (eg, Asp97), whereas AMD3100 associates closer to TM6 (eg, Asp262) (Pándy-Szekeress et al, 2023). Interestingly, the distinct binding orientation of IT1t was postulated to cause monomerization of the CXCR4, as other inverse agonists shared some overlap with the IT1t binding site. No structural information is available for TG-0054 binding to the CXCR4, but molecular docking suggests that it has reasonable overlap with the binding site of AMD3100 (Sukhtankar, 2023b). It would therefore be of interest to explore the binding site of TG-0054 further, to investigate the relationship between its binding site and pharmacological action.

As AMD3100 is successfully used in the clinic for HSC mobilization, inverse agonism of the CXCR4 seems to be dispensable for clinical efficacy. However, constitutive signaling of the CXCR4 might be relevant in other pathophysiological conditions. Elevated, sustained basal signaling of CXCR4 appears to be highly context-dependent and is known to be affected by CXCR4 expression levels and mutations (Salanga et al, 2009; İşbilir et al, 2020). Increased CXCR4 expression levels were detected in, for example, lung, breast, and colorectal cancers, suggesting that such tumor cells might have enhanced constitutive signaling of the CXCR4 (Morein et al, 2020; Smit et al, 2021). Moreover, in a breast cancer model it was shown that an inverse agonist (TN14003) had higher efficacy to attenuate cancer growth than AMD3100 (Lefort et al, 2017). It is therefore

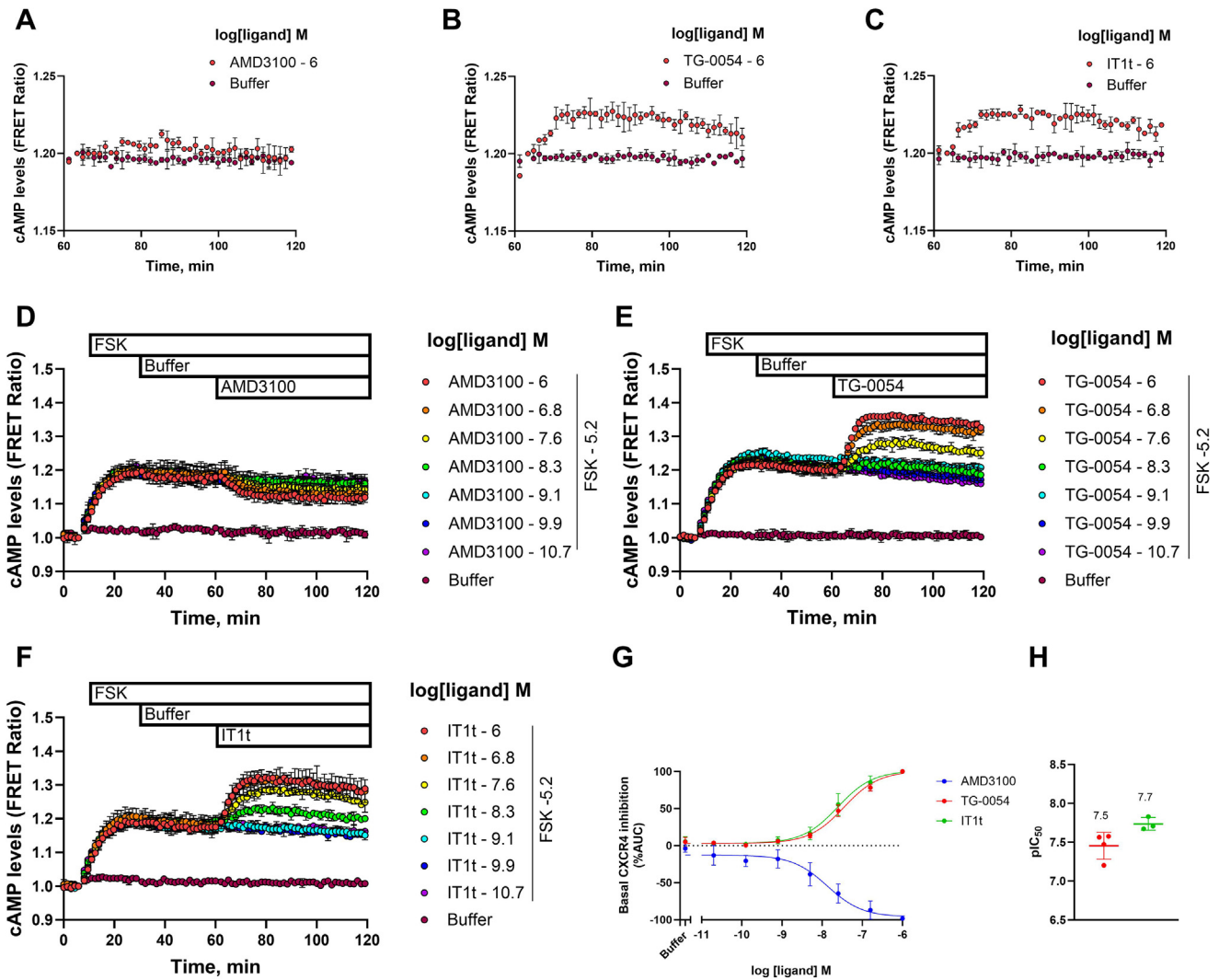


**Fig. 5.** Inverse agonism of TG-0054 at CXCR4 wild-type (WT) and constitutively active mutant CXCR4-N119S. (A–C) HEK293 cells stably expressing the WT CXCR4 and transiently expressing the EPAC FRET sensor on subsequent treatment with FSK ( $6.3 \mu\text{M}$ ) and  $1 \mu\text{M}$ – $2 \text{nM}$  TG-0054, AMD3100, or IT1t. Full curves can be found in [Supplemental Fig. 4](#). (D–F) HEK293 cells transiently expressing the N119S mutant of CXCR4 (CXCR4<sup>N119S</sup>) and EPAC FRET sensor. Cells were exposed to fixed concentrations of FSK ( $t = 8$  minutes, cycle 6), then buffer ( $t = 31$  minutes), followed by increasing concentrations of CXCR4 inhibitor ( $t = 62$  minutes). FRET ratios in panels A–F were calculated as the FRET-donor signal over the FRET-acceptor signal, and the resulting signal is therefore proportional to the level of cAMP levels. (G) Dose-dependent inhibition curves of TG-0054, AMD3100, and IT1t for CXCL12-induced CXCR4<sup>N119S</sup> activity. Data points represent the normalized (buffer = 0%, max. inhibitor conc. = 100%) and pooled mean  $\pm$  SD of AUC ( $t = 63$ – $120$  minutes) from experiments depicted in panels D–F, fitted for illustrative purposes. (H) Comparisons of pIC<sub>50</sub> values determined for TG-0054 and IT1t, with mean  $\pm$  SD depicted. Graphs show representative traces of  $N = 3$  (IT1t) or  $N = 4$  (TG-0054) experiments with 2 technical replicates per experiment.

conceivable that inverse agonists have an advantage over neutral antagonists in attenuating cancer progression.

In conclusion, TG-0054 acted as a potent inhibitor of both constitutive and CXCL12-induced CXCR4 signaling. As TG-0054 was shown here to have unique pharmacological properties, it is a valuable tool for studying the molecular pharmacology of CXCR4. It remains to be seen whether this mechanism of action, clearly distinct from the clinically used AMD3100, will be of therapeutic interest.

## Abbreviations

AUC, area under the curve; BSA, bovine serum albumin; BRET, bioluminescence resonance energy transfer; DMEM, Dulbecco's modified Eagle's medium; EPAC, exchange protein directly activated by cAMP; FRET, Förster resonance energy transfer; FSK, forskolin; GPCR, G protein-coupled receptor; HSC, hematopoietic stem

cell; HTRF, homogeneous time resolved fluorescence; IT1t, Isothiourea-1t; NLuc, NanoLuciferase; PEI, polyethylenimine; ROI, regions of interest; SpIDA, spatial intensity distribution analysis; TB, temporal brightness; TM, transmembrane; YFP, yellow fluorescent protein.

## Acknowledgments

We thank to N. Dobberstein for making the CXCR4+EPAC stable cell line.

## Financial support

This research was funded by a European Union's Horizon2020 MSCA Program (Grant agreement 860229 [ONCOR-NET2.0]), and C.P. was funded under the same program [Grant agreement 101063969]. Finally, N.B. and S.M. were funded by

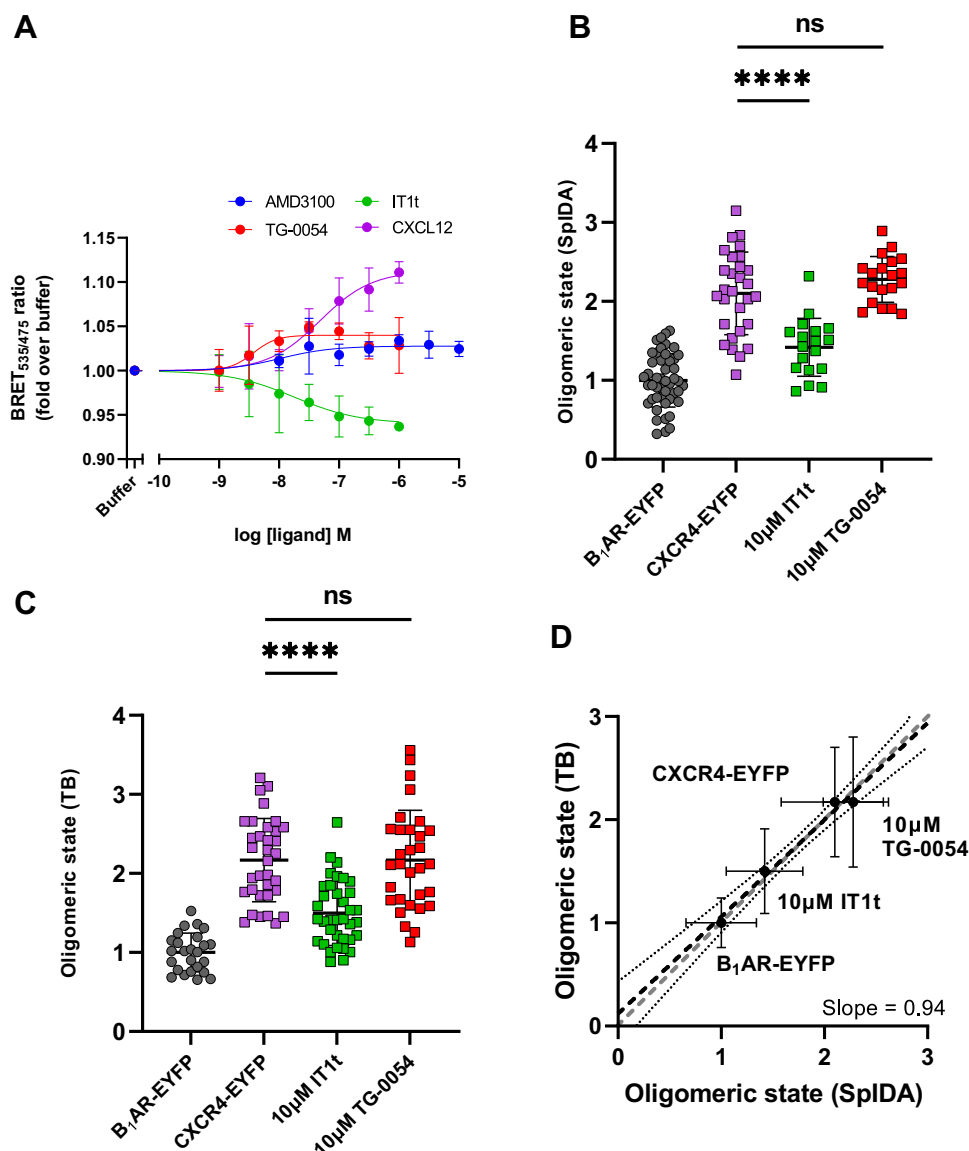


**Fig. 6.** TG-0054 does not disrupt CXCR4 oligomers, in contrast to IT1t. (A) BRET ratio of Rluc- and YFP-tagged CXCR4 following the exposure of CXCL12, AMD3100, IT1t, and TG-0054 at increasing concentrations for 15 minutes, data points are mean  $\pm$  SD, displayed as fold over basal, fitted for illustrative purposes. Spatial (B) and temporal (C) brightness analysis of CXCR4-EYFP oligomeric states following 10  $\mu$ M TG-0054 or IT1t exposure for 30 minutes, each data point represents the average molecular brightness from one sample image with multiple cells, choosing at least 6 different ROIs normalized to the monomeric control  $\beta_1$ AR, mean  $\pm$  SD of  $N = 3$  experiments. Representative images can be found in [Supplemental Fig. 5](#). Statistical analysis was done with the one-way ANOVA test followed post hoc by Tukey's multiple pairwise comparison ( $P < .0001$ ). (D) Correlation plot of spatial and temporal brightness results with SD error bars.

the Netherlands Organization for Scientific Research (NWO) [Grant agreement 881 ENPPS.TA.019.003].

### Conflict of interest

Aurélien Rizk is the CSO of InterAx Biotech AG; Kylie S. Pan, Susanne Roth, and Mirjam Zimmermann were affiliated to InterAx Biotech AG during the period in which the research in this paper was carried out.

### Data availability

Data and reagents generated for and reported on in this study will be made available upon request. Authors declare that all the data supporting this study are included within this manuscript and in the [supplemental materials](#).

### Authorship contributions

*Participated in research design:* Pan, Wang, Bergkamp, Mobach, Annibale, Siderius, Zimmermann, Smit, Bosma.

*Conducted experiments:* Pan, Wang, Pfeil, Bergkamp, Mobach.

*Contributed new reagents or analytic tools:* Annibale.

*Performed data analysis:* Pan, Wang, Pfeil, Bergkamp.

*Wrote or contributed to the writing of the manuscript:* Pan, Wang, Pfeil, Bergkamp, Mobach, Roth, Rizk, Lohse, Annibale, Siderius, Zimmermann, Smit, Bosma.

### Supplemental material

This article has supplemental material available at [molpharm.aspetjournals.org](https://molpharm.aspetjournals.org).

## References

- Agle KA, Vongsa RA, and Dwinell MB (2010) Calcium mobilization triggered by the chemokine CXCL12 regulates migration in wounded intestinal epithelial monolayers. *J Biol Chem* **285**:16066–16075.
- Annibale P and Lohse MJ (2020) Spatial heterogeneity in molecular brightness. *Nat Methods* **17**:273–275.
- Bachelier F, Ben-Baruch A, Burkhardt AM, Charo IF, Combadiere C, Farber JM, Förster R, Graham GJ, Hills R, Horuk R, et al (2014) International union of pharmacology. LXXXIX. Update on the extended family of chemokine receptors and introducing a new nomenclature for atypical chemokine receptors. *Pharmacol Rev* **66**:1–79.
- Bachelier F, Ben-Baruch A, Burkhardt AM, Charo IF, Combadiere C, Farber JM, Förster R, Graham GJ, Hills R, Horuk R, et al (2020) Chemokine receptors (version 2020.5) in the IUPHAR/BPS Guide to Pharmacology Database. *IUPHAR/BPS Guide to Pharmacology CITE* **2020**.
- Benkel T, Zimmermann M, Zeiner J, Bravo S, Merten N, Lim VJY, Matthees ESF, Drube J, Miess-Tanneberg E, Malan D, et al (2022) How carvedilol activates  $\beta_2$ -adrenoceptors. *Nat Commun* **13**:7109.
- Bergkamp ND, van Senten JR, Brink HJ, Belbelman MP, van den Bor J, Çobanoğlu TS, Dinkla K, Köster J, Klau G, Siderius M, et al (2023) A virally encoded GPCR drives glioblastoma through feed-forward activation of the SK1-S1P1 signaling axis. *Sci Signal* **16**:eade6737.
- Brillet K, Kieffer BL, and Massotte D (2003) Enhanced spontaneous activity of the mu opioid receptor by cysteine mutations: characterization of a tool for inverse agonist screening. *BMC Pharmacol* **3**:14.
- Chung DT, Chang L-W, Huang Y-H, Tsai C-Y, Hsu C-H, King C-HR, Yuan JH, Yen C-F, Chen Y-M, Lu YC, et al (2009) TG-0054, a novel and potent stem cell mobilizer, displays excellent PK/PD and safety profile in phase I trial. *Blood* **114**, 866–866.
- Copelan EA (2006) Hematopoietic stem-cell transplantation. *N Engl J Med* **354**:1813–1826.
- Fiorina P, Jurewicz M, Vergani A, Petrelli A, Carvello M, D'Addio F, Godwin JG, Law K, Wu E, Tian Z, et al (2011) Targeting the CXCR4–CXCL12 axis mobilizes autologous hematopoietic stem cells and prolongs islet allograft survival via programmed death ligand 1. *J Immunol* **186**:121–131.
- Fricker SP (2013) Physiology and pharmacology of plerixafor. *Transfus Med Hemother* **40**:237–245.
- García-Cuesta EM, Martínez P, Selvaraju K, Gómez Pozo AM, D'Agostino G, Gardeta S, Quijada-Freire A, Blanco Gabella P, Roca C, Jiménez-Saiz R, et al (2024) Allosteric modulation of the CXCR4: CXCL12 axis by targeting receptor nanoclustering via the TMV-TMVI domain. *ELife* **3**:RP93968.
- Harms M, Gilg A, Ständker L, Beer AJ, Mayer B, Rasche V, Gruber CW, and Münch J (2020) Microtiter plate-based antibody-competition assay to determine binding affinities and plasma/blood stability of CXCR4 ligands. *Sci Rep* **10**:16036.
- Heuninck J, Perpiñá Viciano C, İşbilir A, Caspar B, Capoferri D, Briddon SJ, Durroux T, Hill SJ, Lohse MJ, Milligan G, et al (2019) Context-dependent signaling of CXC chemokine receptor 4 and atypical chemokine receptor 3. *Mol Pharmacol* **96**:778–793.
- Hsu W-T, Jui H-Y, Huang Y-H, Su M-YM, Wu Y-W, Tseng W-YI, Hsu M-C, Chiang B-L, Wu KK, and Lee C-M (2015) CXCR4 antagonist TG-0054 mobilizes mesenchymal stem cells, attenuates inflammation, and preserves cardiac systolic function in a porcine model of myocardial infarction. *Cell Transplant* **24**:1313–1328.
- Hsu W-T, Lin C-H, Jui H-Y, Tseng Y-H, Shun C-T, Hsu M-C, Wu KK-Y, and Lee C-M (2018) CXCR4 antagonist reduced the incidence of acute rejection and controlled cardiac allograft vasculopathy in a swine heart transplant model receiving a mycophenolate-based immunosuppressive regimen. *Transplantation* **102**:2002–2011.
- İşbilir A, Möller J, Arimont M, Bobkov V, Perpiñá-Viciano C, Hoffmann C, Inoue A, Heukers R, de Graaf C, Smit MJ, et al (2020) Advanced fluorescence microscopy reveals disruption of dynamic CXCR4 dimerization by spocket-specific inverse agonists. *Proc Natl Acad Sci U S A* **117**:29144–29154.
- İşbilir A, Serfling R, Möller J, Thomas R, De Faveri C, Zabel U, Scarselli M, Beck-Sickingler AG, Bock A, Coin I, et al (2021) Determination of G-protein-coupled receptor oligomerization by molecular brightness analyses in single cells. *Nat Protoc* **16**:1419–1451.
- Kang Y, Chen BJ, Deoliveira D, Mito J, and Chao NJ (2010) Selective enhancement of donor hematopoietic cell engraftment by the CXCR4 antagonist AMD3100 in a mouse transplantation model. *PLoS One* **5**:e11316.
- Karpova D and Bonig H (2015) Concise review: CXCR4/CXCL12 signaling in immature hematopoiesis—lessons from pharmacological and genetic models. *Stem Cells* **33**:2391–2399.
- Kazemi Z, Bergmayr C, Prchal-Murphy M, Javaheri T, Themanns M, Pham HT, Strohmaier W, Sexl V, Freissmuth M, and Zebedin-Brandl E (2016) Repurposing treprostinil for enhancing hematopoietic progenitor cell transplantation. *Mol Pharmacol* **89**:630–644.
- Lao J, He H, Wang X, Wang Z, Song Y, Yang B, Ullahkhan N, Ge B, and Huang F (2017) Single-molecule imaging demonstrates ligand regulation of the oligomeric status of CXCR4 in living cells. *J Phys Chem B* **121**:1466–1474.
- Lefort S, Thuleau A, Kieffer Y, Sirven P, Bieche I, Marangoni E, Vincent-Salomon A, and Mehta-Grigoriou F (2017) CXCR4 inhibitors could benefit to HER2 but not to triple-negative breast cancer patients. *Oncogene* **36**:1211–1222.
- Martínez-Muñoz L, Rodríguez-Frade JM, Barroso R, Sorzano CÓS, Torreño-Pina JA, Santiago CA, Manzo C, Lucas P, García-Cuesta EM, Gutierrez E, et al (2018) Separating actin-dependent chemokine receptor nanoclustering from dimerization indicates a role for clustering in CXCR4 signaling and function. *Mol Cell* **70**:106–119.e10.
- Mathiesen JM, Vedel L, and Bräuner-Osborne H (2013) Camp biosensors applied in molecular pharmacological studies of G protein-coupled receptors. *Methods Enzymol* **522**:191–207.
- Moll NM and Ransohoff RM (2010) CXCL12 and CXCR4 in bone marrow physiology. *Expert Rev Hematol* **3**:315–322.
- Moren D, Erlichman N, and Ben-Baruch A (2020) Beyond cell motility: the expanding roles of chemokines and their receptors in malignancy. *Front Immunol* **11**:952.
- Murdoch C (2000) CXCR4: Chemokine receptor extraordinaire. *Immunol Rev* **177**:175–184.
- Nijmeijer S, Engelhardt H, Schultes S, Van De Stolpe AC, Lusink V, De Graaf C, Wijtmans M, Haaksma EE, De Esch JJ, Stachurski K, et al (2013) Design and pharmacological characterization of VUF14480, a covalent partial agonist that interacts with cysteine 983.36 of the human histamine H4 receptor. *Br J Pharmacol* **170**:89–100.
- Núñez RE, Del Valle MM, Ortiz K, Almodovar L, and Kucheryavykh L (2021) Microglial cytokines induce invasiveness and proliferation of human glioblastoma through Pyk2 and FAK activation. *Cancers* **13**:6160.
- Orsini MJ, Parent JL, Mundell SJ, Marchese A, and Benovic JL (1999) Trafficking of the HIV coreceptor CXCR4. Role of arrestins and identification of residues in the C-terminal tail that mediate receptor internalization. *J Biol Chem* **274**:31076–31086.
- Pándy-Szekeress G, Caroli J, Mamyrbekov A, Kermani AA, Keserü GM, Kooistra AJ, and Gloriam DE (2023) GPCRdb in 2023: states-specific structure models using AlphaFold2 and new ligand resources. *Nucleic Acids Res* **51**:D395–D402.
- Paradis JS, Feng X, Murat B, Jefferson RE, Sokrat B, Szpakowska M, Hogue M, Bergkamp ND, Heydenreich FM, Smit MJ, et al (2022) Computationally designed GPCR quaternary structures bias signaling pathway activation. *Nat Commun* **13**:6826.
- Percherancier Y, Berchiche YA, Slight I, Volkmer-Engert R, Tamamura H, Fujii N, Bouvier M, and Heveker N (2005) Bioluminescence resonance energy transfer reveals ligand-induced conformational changes in CXCR4 homo- and heterodimers. *J Biol Chem* **280**:9895–9903.
- Rosenberg EM, Harrison RE, Tsou LK, Drucker N, Humphries B, Rajasekaran D, Luker KE, Wu C-H, Song J-S, Wang C-J, et al (2019) Characterization, dynamics, and mechanism of CXCR4 antagonists on a constitutively active mutant. *Cell Chem Biol* **26**:662–673.e7.
- Salanga CL, O'Hayre M, and Handel T (2009) Modulation of chemokine receptor activity through dimerization and crosstalk. *Cell Mol Life Sci* **66**:1370–1386.
- Schuster MW, Hagog N, Jalilzeinali B, Funkhauser S, Yohannan MS, Sadler J, Wood S, Carey S, Kelleher K, Tsai C-E, et al (2013) Rapid mobilization of CD34+ progenitor cells with TG0054-03, a novel CXC chemokine receptor 4 (CXCR4) antagonist. *Blood* **122**:905.
- Smit MJ, Schlecht-Louf G, Neves M, van den Bor J, Penela P, Siderius M, Bachelier F, and Mayor F (2021) The CXCL12/CXCR4/ACKR3 axis in the tumor microenvironment: signaling, crosstalk, and therapeutic targeting. *Annu Rev Pharmacol Toxicol* **61**:541–563.
- Sukhtankar DD, Chang L-W, Tsai C-Y, Cardarelli PM, and Caculitan NG (2023a) Pharmacokinetics and pharmacodynamics of Burixafor hydrobromide (GPC-100), a novel C-X-C chemokine receptor 4 antagonist and mobilizer of hematopoietic stem/progenitor cells, in mice and healthy subjects. *Clin Pharmacol Drug Dev* **12**:1114–1120.
- Sukhtankar DD, Fung JJ, Kim M-N, Cayton T, Chiou V, Caculitan NG, Zalicki P, Kim S, Jo Y, Kim S, et al (2023b) GPC-100, a novel CXCR4 antagonist, improves in vivo hematopoietic cell mobilization when combined with propranolol. *PLoS One* **18**:e0287863.
- Wade SM, Lan K-L, Moore DJ, and Neubig RR (2001) Inverse agonist activity at the  $\alpha_2$ -adrenergic receptor. *Mol Pharmacol* **59**:532–542.
- Wan Q, Okashah N, Inoue A, Nehmé R, Carpenter B, Tate CG, and Lambert NA (2018) Mini G protein probes for active G protein-coupled receptors (GPCRs) in live cells. *J Biol Chem* **293**:7466–7473.
- Ward RJ, Pediani JD, Marsango S, Jolly R, Stoneman MR, Biener G, Handel TM, Raicu V, and Milligan G (2021) Chemokine receptor CXCR4 oligomerization is disrupted selectively by the antagonist ligand IT1t. *J Biol Chem* **296**:100139.
- Yen YC, Schafer CT, Gustavsson M, Eberle SA, Dominik PK, Denek D, Zhang P, Schall TJ, Kossiakoff AA, Tesmer JGG, et al (2022) Structures of atypical chemokine receptor 3 reveal the basis for its promiscuity and signaling bias. *Sci Adv* **8**:eabn8063.
- Zhang W-B, Navenot J-M, Haribabu B, Tamamuraz H, Hiramatu K, Omagari A, Pei G, Manfredi JP, Fujii N, Broach JR, et al (2002) A point mutation that confers constitutive activity to CXCR4 reveals that T140 is an inverse agonist and that AMD3100 and ALX40-4C are weak partial agonists. *J Biol Chem* **277**:24515–24521.